PNAS RESEARCH ARTICLE | APPLIED PHYSICAL SCIENCES

The onset of heterogeneity in the pinch-off of suspension drops

Virgile Thiévenaz[a] and Alban Sauret[a,1]

Edited by David Weitz, Harvard University, Cambridge, MA; received November 16, 2021; accepted February 13, 2022

At large scales, particulate suspensions flow like homogeneous viscous liquids, but at the particle scale, the role of the local heterogeneity brought by the particles cannot be neglected. The volume fraction also matters; in dense suspensions, particulate effects can be felt across distances much larger than the particle diameter. Therefore, whether a suspension should behave as a homogeneous or heterogeneous fluid is a matter of scale. Here, we consider the canonical situation of the pinch-off of suspension drops to study the behavior of suspensions at different scales. Initially, the filament of suspension thins down like a homogeneous liquid until reaching a critical thickness at which the thinning accelerates. Eventually, a region devoid of particles appears, and the breakup occurs similarly to a homogeneous viscous liquid. Although this problem have been studied for almost 20 y, the role of heterogeneity in the acceleration of the pinch-off is still not understood. We show that the onset of heterogeneity corresponds to the dislocation of the suspensions where local fluctuations in particle concentration increase. We derive scaling laws for the dynamics in the heterogeneous regime and develop a model to predict the coherence length at which the discrete nature of the particles appears, and we demonstrate that this length depends both on the particle size and on the volume fraction of the suspension. We extend this approach to polydisperse suspensions. Our work sheds light on the mesoscopic scale below which starts the heterogeneous regime and a continuum approach is not valid anymore.

pinch-off | suspensions | interface | singularity | heterogeneity

Significance

The pinch-off of a liquid drop extruded from a nozzle is a canonical situation that involves a series of self-similar regimes ending in a finite-time singularity. This configuration allows for exploring capillary flows over a large range of scales. In the case of suspension drops, the presence of particles breaks the self-similarity by introducing a length scale that can be much larger than the particle diameter. This length scale is a signature of the heterogeneities and delimitates a regime, in which a continuum approach of a suspension can be used from a regime where the discrete nature of the particles is involved.

Suspensions are ambivalent fluids. Depending on the length scale at which they flow, they can be considered homogeneous or heterogeneous. At length scales much larger than the particle size, a suspension behaves like an effective viscous liquid whose viscosity $\eta(\phi)$ increases with the volume fraction of particles ϕ (1). However, below a certain length scale, fluctuations of particle concentration can strongly influence the flow, and the heterogeneous nature of the particles plays a crucial role. This change of scale naturally occurs during the breaking of a liquid into droplets; as a drop detaches from a nozzle, the neck that binds the drop to the nozzle thins down and eventually vanishes (2–4). In the capillary regime, the thickness of this liquid neck $h(t)$ may undergo different self-similar regimes (5). If the flow is capillary inertial, $h(t) \sim (\gamma/\rho)^{1/3}(t_c - t)^{2/3}$; if the flow is capillary viscous, $h(t) \sim \gamma(t_c - t)/\eta$. The neck finally breaks up in a finite-time singularity at time t_c.

In practical applications, the atomized fluids can be suspensions containing dispersed particles. For example, in inkjet printing (6, 7), biofluids printing (8), and spray-painting, the fluids contain solid objects that may be rigid (pigments) or not (cells) as well as polymers and other solutes. Therefore, as a liquid neck of such complex fluids thins down, its thickness successively goes through the length scales of each component. This reveals the heterogeneous nature of the fluid; the aforementioned self-similar regimes disappear and make way for thinning regimes that are specific of the components. A well-known example is the thinning of a thread of dilute polymer solution (9); initially, the liquid neck thins down like an inviscid Newtonian fluid, following the power law $h(t) \propto (t_c - t)^{2/3}$. At a certain point, the polymer starts interacting with the flow, and the thickness $h(t)$ decreases exponentially with time. Adding solid particles to the polymer solution does not result in a new thinning regime, but it significantly changes the threshold from one regime to another (10).

Understandably, the complexity of the problem drastically increases with the number of components because it implies an increase of the number of length scales. Also, each kind of component (particles, polymers, cells, etc.) may exist in a range of sizes. To allow for a physical insight, we must narrow the focus to a single kind of component. Therefore, in order to isolate the viscous effects in the pinch-off of complex fluid drops, we investigate non-Brownian, neutrally buoyant particles dispersed in a viscous liquid.

The seminal work of Furbank and Morris (11) on the pinch-off of suspension drops revealed a two-step mechanism. The particles are initially homogeneously distributed in

Author affiliations: [a]Department of Mechanical Engineering, University of California, Santa Barbara, CA 93106

Author contributions: V.T. and A.S. designed research; V.T. and A.S. performed research; V.T. and A.S. analyzed data; A.S. supervised the project; and V.T. and A.S. wrote the paper.

The authors declare no competing interest.

This article is a PNAS Direct Submission.

[1]To whom correspondence may be addressed. Email: asauret@ucsb.edu.

This article contains supporting information online at https://www.pnas.org/lookup/suppl/doi:10.1073/pnas.2120893119/-/DCSupplemental.

Published March 23, 2022.

the neck. Then, when the neck has thinned down to a few particle diameters, the particle volume fraction ϕ fluctuates. It was later shown that the homogeneous regime is similar to the thinning of a viscous liquid of matching viscosity (12, 13). At some point, the velocity profile in the neck becomes discontinuous (14), and the thinning accelerates (15). This transition from the homogeneous regime to the heterogeneous regime during the generation of suspension drops occurs at a critical thickness that increases with the particle diameter d but that is not necessarily of the same order of magnitude (12). After some time, the neck becomes thinner than the particle diameter and reduces to the interstitial liquid (16). For bidisperse suspensions, the transition depends on the relative fraction of each size of particles; the more large particles there are, the earlier the heterogeneous regime is (17).

Past studies have suggested that the heterogeneous regime observed may be due to shear thickening (18, 19) or to jamming in the neck (20). However, these explanations are incompatible with the dilute and semidilute cases, in which even one single particle is sufficient to trigger the acceleration of the pinch-off (14). It was reported that concentration fluctuations were amplified by the curvature gradient at the neck (21). Unfortunately, capillary effects alone cannot explain why the heterogeneous regime starts at thicknesses much larger than the particle diameter (12, 22). Accordingly, the present study aims to unify the different descriptions of suspension drop pinch-off and to clarify the role of solid heterogeneities on drop formation.

The transition to a heterogeneous regime where the particles impact the dynamics beyond a simple increase in viscosity is not specific to the pinch-off of suspension drop. Such behavior has also been reported for other flows of suspensions, dip coating (23, 24), inclined plane (22), drop impact and sheet spreading (26), jet of suspensions (27), or spreading of a contact line (28). In all of these situations, the suspensions are found to behave either like homogeneous viscous liquids or like heterogeneous media. The passage from one regime to another occurs at a specific length scale, which can be much larger than the particle diameter d and depends on the volume fraction ϕ and d. In *Discussion*, we use the results of the pinch-off dynamics to conceptualize the onset of heterogeneity in free surface flows of suspensions.

We study the pinch-off of drops of suspensions: first, monodisperse and then, polydisperse. By considering the stability of a concentration fluctuation at the neck, we identify a specific thinning regime that we call the dislocation of the suspension. We derive scaling laws that describe this accelerated regime and its duration; these scaling laws match experiments conducted with a wide range of particle diameters and volume fractions up to $\phi = 50\%$ and are applicable to monodisperse and polydisperse suspensions. Moreover, applying this approach to results from the literature (13, 18, 19, 29) enables a global vision of the pinch-off mechanisms of drops of non-Brownian suspensions.

Thinning Dynamics

Fig. 1 shows examples of the pinch-off of drops with the pure silicone oil, further used as interstitial liquid, and suspensions of particles of diameter $d = 140\mu$m and increasing volume fractions $\phi = 2\%$, $\phi = 20\%$, and $\phi = 50\%$. The influence of the diameter of the particles composing the suspension is also illustrated for a volume fraction of $\phi = 50\%$ and particles of diameters 20 and 250-μm. In the absence of particles (i.e., for the interstitial fluid only), the pinch-off dynamics illustrated in Fig. 1*A* shows that the neck that binds the drop to the nozzle thins down as gravity and capillary pressure pull on it and stretches into a long filament. Eventually, the thinning accelerates in the region where this filament connects to the nozzle, leading to the breakup of the filament.

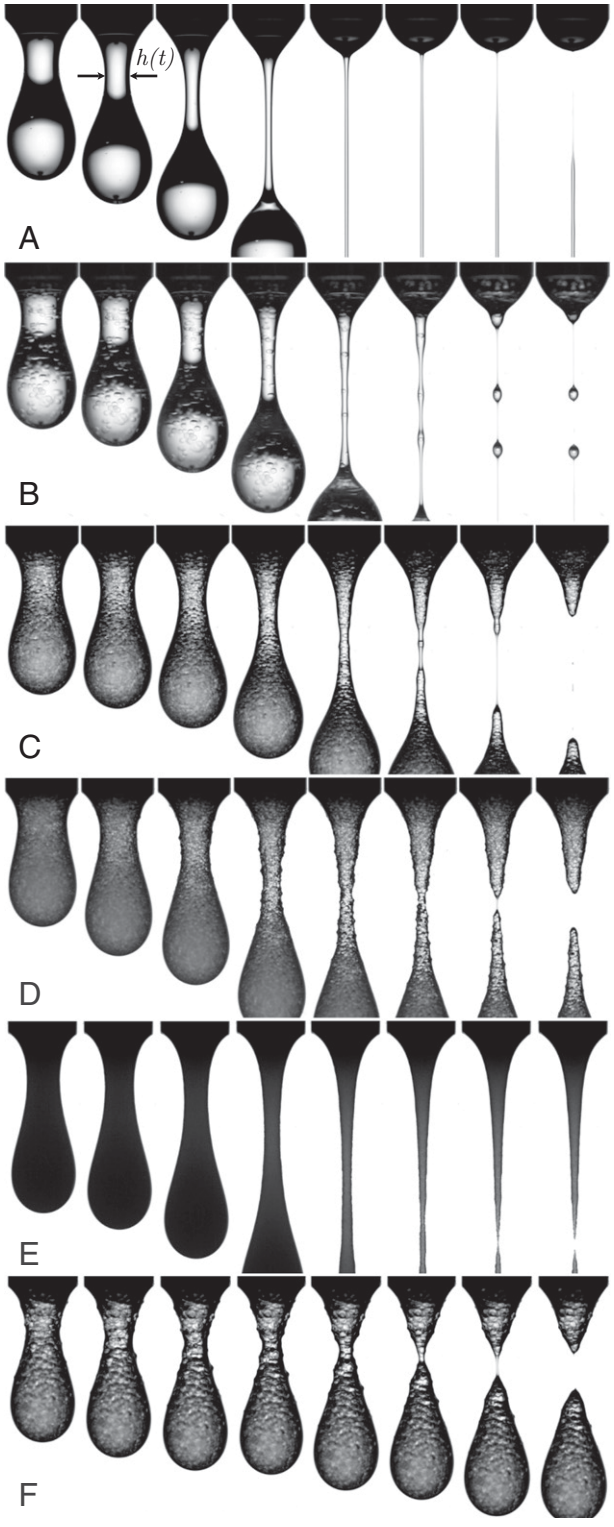

Fig. 1. Time series of the pinch-off of drops of (*A*) interstitial liquid (silicone oil, no particles); (*B*) $\phi = 2\%$, (*C*) $\phi = 20\%$, and (*D*) $\phi = 50\%$ of $d = 140\mu$m particles; (*E*) $\phi = 50\%$ of $d = 20\mu$m particles; and (*F*) $\phi = 50\%$ of $d = 250\mu$m particles. The nozzle has an outer diameter of 2.75 mm and serves as a scale bar (Movies S1–S6 and *SI Appendix*).

The initial thinning dynamics of the particulate suspensions is similar to the pure Newtonian liquid, although the dynamics is much slower due to the increase in viscosity induced by the presence of particles. In the dilute regime, $\phi = 2\%$ shown in

Fig. 1*B*, the neck stretches into a slender filament, similarly to the pure liquid case, but this filament is eventually disturbed by the particles. Each particle trapped in the filament leads to the formation of a satellite drop, typically when the thickness of the filament is comparable with the particle size. The satellite drops are separated by viscous filaments that thin down with an associated dynamics similar to the pure liquid case. At moderate volume fraction (e.g., $\phi = 20\%$ illustrated in Fig. 1*C*), the particles begin to slightly deform the liquid–air interface before they are pulled apart. Eventually, a thin filament free of particles connects the drop to the rest of the liquid at the nozzle. The resulting long filament of interstitial liquid is much thinner than the particle size and free of particles.

For dense suspensions, here $\phi = 50\%$ in Fig. 1 *D*–*F*, the neck breaks faster, and the pinch-off dynamics depends on the particle diameter. For the 20-μm particles, illustrated in Fig. 1*E*, the neck stretches significantly, but its shape is very different from the pure liquid case. The thinning dynamics with large particles is highly accelerated, as illustrated with the 250-μm particles shown in Fig. 1*F*. In all three dense cases shown here, the penultimate picture reveals a very short time during which the neck is made of interstitial liquid only. However, the length of this filament without particles is much shorter than the one observed for smaller volume fractions. Another significant difference during the pinch-off dynamics is the location where the breakup occurs. Indeed, the viscous liquid always breaks up near the nozzle at the top of the filament, whereas all suspensions break farther away from the nozzle, especially for small particles. Also, the thinning of suspensions is a localized phenomenon as shown by image cross-correlation that enables us to estimate the distance over which the velocity profile evolves (*SI Appendix*). We find the velocity gradient to be negligible outside the volume h^3 around the neck (14).

At each time step, we extract the thickness of the neck at the thinnest point h (Fig. 1*A*). The pinch-off of the neck occurs at a finite-time $t = t_c$, and we thus consider the time to pinch-off, $t_c - t$. Fig. 2*A* reports the thinning dynamics $h(t) = f(t_c - t)$ of suspensions of 140-μm particles of volume fractions ϕ ranging from 2% (purple) to 50% (yellow) in real time in Fig. 2*A* and in rescaled time in Fig. 2*B*. In all plots, the time elapses from right to left. For comparison, we reported in black the thinning dynamics of the pure liquid without particles.

For the most dilute suspensions ($\phi = 2\%$; in purple), the dynamics is barely distinguishable from that of the pure liquid. The difference appears as soon as the volume fraction is larger than 10%, where the thinning dynamics observed is slower. More generally, the larger the volume fraction ϕ of the suspension, the longer the thinning is, and the later the pinch-off is. However, the shape of the thinning dynamics also changes with the volume fraction. For the most concentrated suspensions used here ($\phi = 50\%$; in yellow), the dynamics is slower but continuously accelerated. Thus, the thinning of the suspension is not simply faster but intrinsically different and driven by a different physical mechanism.

Bonnoit et al. (12) have shown that down to a certain neck thickness, a particulate suspension behaves like a homogeneous liquid of matching viscosity. In addition, the thinning dynamics of the suspension can be rescaled onto the dynamics of another viscous liquid (17). The method consists of stretching the time to pinch-off by a factor α_η and shifting it by the duration Δt, thus changing $t_c - t$ to $\alpha_\eta(t_c - t) + \Delta t$. For each suspension used in this study, we compute the values of α_η and Δt so that the early thinning dynamics of the suspension collapses onto the dynamics of the interstitial liquid. Fig. 2*B* shows the rescaled thinning dynamics obtained with this method when varying the particle volume fraction ϕ. Once the proper rescaling is applied, the thinning dynamics for suspensions of varying volume fraction collapses onto that of a homogeneous fluid, and the two dynamics match down to a critical thickness $h^\star$, which depends on the particle size and the volume fraction. When the neck becomes thinner than $h^\star$, the thinning of the suspension accelerates and becomes faster than for the equivalent liquid, as can be seen in Fig. 2*B*.

The specific dynamics of the suspension when $h < h^\star$ is itself divided into two regimes, as illustrated in logarithmic scale in Fig. 2*C* for a suspension of volume fraction $\phi = 40\%$ and particle size $d = 140\mu$m. Below the critical thickness $h^\star$, there are two well-defined regimes, each captured by a different power law $h(t) \sim (t_c - t)^\alpha$. The latest regime, in which h decreases linearly with time, is the viscous-capillary regime known for the pinch-off of viscous liquids (30, 31). The experiments reveal that there are no particles in the neck anymore at this time. The experimental thinning rate in this case is $h(t)/(t_c - t) = 0.08\,\mathrm{m} \times \mathrm{s}^{-1}$, and the theoretical thinning rate (30) is $0.0304\gamma/\eta_f = 0.066\,\mathrm{m} \times \mathrm{s}^{-1}$

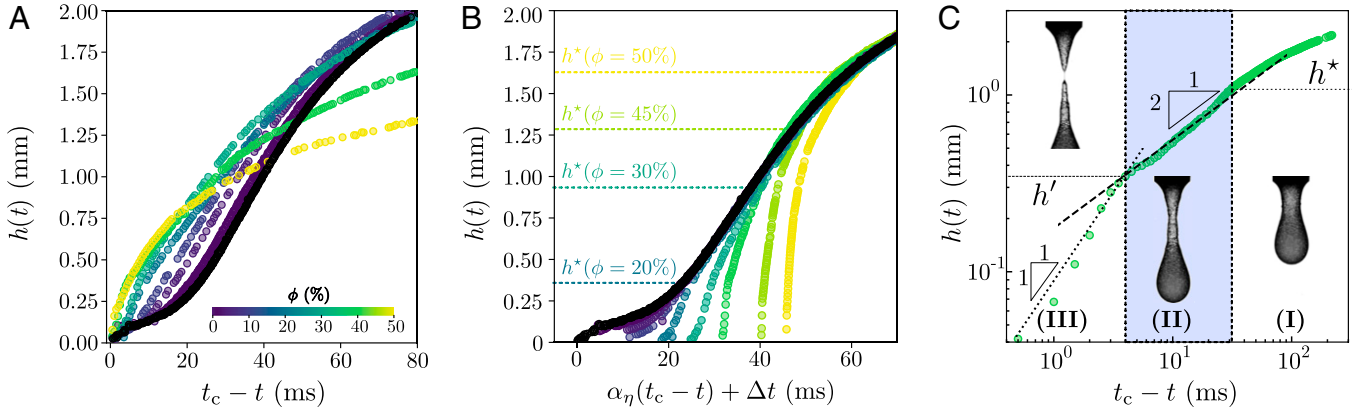

Fig. 2. (*A*) Thinning dynamics of suspensions of 140-μm particles dispersed in silicone oil at various volume fractions ϕ (colored symbols). The black symbols represent the dynamics of the interstitial fluid ($\phi = 0$). (*B*) Thinning dynamics in rescaled time. For each suspension, the time to pinch-off $t_c - t$ is shifted and stretched into $\alpha_\eta(t_c - t) + \Delta t$, so that the dynamics overlaps with that of the interstitial fluid in the early thinning regime. The dynamics of the suspensions deviate from the interstitial liquid and accelerate at the critical thickness $h = h^\star$, represented by the horizontal dashed lines for volume fractions $\phi = 20$, 30, 45, and 50%. (*C*) Thinning dynamics in logarithmic scale for $\phi = 40\%$ and $d = 140\mu$m. The neck undergoes three successive thinning regimes: (I) the homogeneous liquid regime; (II) the dislocation, where $h(t) \sim (t_c - t)^{1/2}$; and (III) the interstitial regime, where $h(t) \sim t_c - t$, similarly to a viscous liquid.

(η_f denotes the viscosity of the interstitial fluid), which is slightly smaller but in good agreement with our measurement. Therefore, we can define a threshold thickness, h', below which particles do not influence the detachment of the drop anymore. The existence of the two thresholds $h^\star$ and h' leads to the definition of three regimes, shown in Fig. 2*C*: (I) for $h(t) > h^\star$, an equivalent liquid regime, in which the suspension behaves like a homogeneous liquid of matching viscosity; (II) for $h' < h(t) < h^\star$, a dislocation regime, during which the heterogeneity of the suspension plays a crucial role; and (III) for $h(t) < h'$, the interstitial regime, in which the neck is devoid of particles and the thinning is simply the thinning of the interstitial regime. Also, the transition from (I) to (II) corresponds to a change in the evolution of the shape of the drop; for $h > h^\star$, the whole drop deforms, and for $h < h^\star$, only the neck does (*SI Appendix*). The entry into the dislocation regime marks the onset of heterogeneity, where the discrete nature of the particles affects the dynamics beyond simply increasing the macroscopic viscosity.

Onset of Heterogeneity

Thinning Dynamics. Deforming a dense suspension leads to the rearrangement of the particles, which causes dissipation. The local volume fraction of particles remains constant if the particles are simply sliding or rolling along each other and fluctuates if they move away or toward each other. We hypothesize that the detachment of a suspension drop accelerates because particles start moving away from each other in the vicinity of the neck and refer to this phenomenon as the dislocation of the suspension ligament. The word dislocation is not to be taken in its meaning of defect in a lattice, for there is no order in the suspension, but is to be taken in its etymological meaning of sudden separation. The dislocation mechanism begins when pulling particles apart becomes energetically favorable compared with rearranging them. In other words, dislocation is the growth of local fluctuations of the particle volume fraction.

To describe the dislocation regime, we consider a liquid film of thickness a between two portions of suspension, which represents the local fluctuation of concentration in the neck. The viscosity of the suspension is denoted η; the viscosity of the interstitial liquid is denoted η_f. Pulling the two portions apart at the velocity $\dot{a}$ dissipates the power $\eta_f h^4 \dot{a}^2/a^3$ (*Materials and Methods*). We assume that during the dislocation regime, a is of the order of magnitude of the particle diameter so that $a \sim d$. By balancing the power associated with the capillary forces $\gamma h^2/(t_c - t)$ and the power associated with the viscous dissipation, we obtain the scaling law for the thinning dynamics in the dislocation regime:

$$h(t) \sim (t_c - t)^{1/2} \sqrt{\frac{\gamma}{\eta_f} d}. \qquad [1]$$

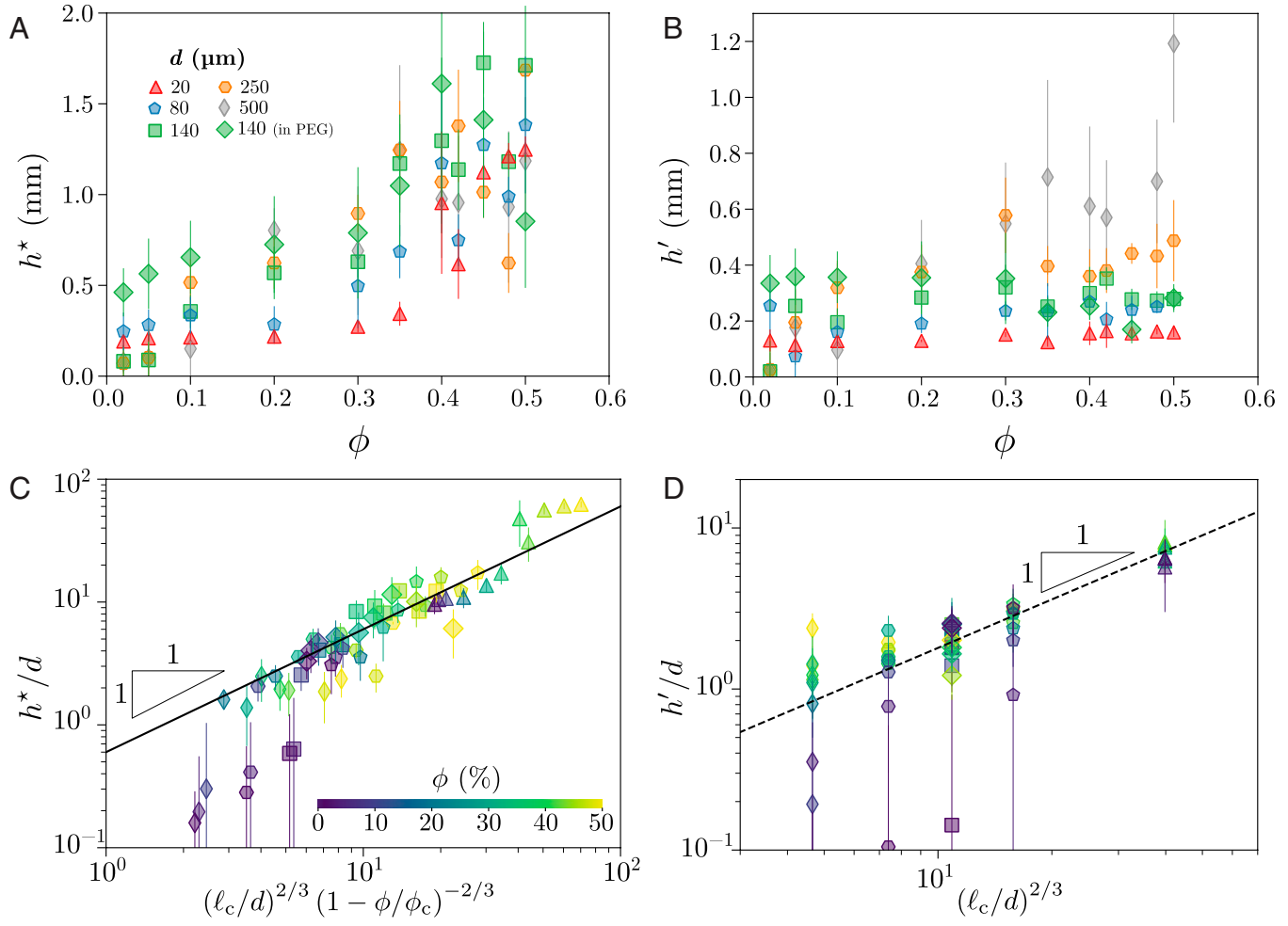

Fig. 3. Critical thickness (*A*) at the transition between the equivalent fluid regime (I) and the dislocation regime (II), $h^\star$, and (*B*) at the transition between the dislocation regime (II) and the interstitial regime (III), h', as a function of the volume fraction ϕ for monodisperse suspensions. (*C*) $h^\star/d$ and (*D*) h'/d plotted following the predictions given by Eqs. **2** and **3**, respectively. The different symbols represent different particle sizes, and the big diamonds represent experiments conducted with PEG. In *C* and *D*, the colors represent the volume fraction from dilute (2%; purple) to dense (50%; yellow), and the lines have a slope of one.

Eq. **1** describes the evolution of the thickness of the neck as the capillary pressure makes particles move away from each other and captures well the dynamics in the regime (II) shown in Fig. 2*C*. We systematically observed this scaling law in all of our experiments for suspensions with volume fraction $\phi \geq 20\%$. For dilute-enough suspensions, there is a range of volume fractions in which the thinning of the neck shifts directly from the equivalent regime (I) to the interstitial regime (III). Therefore, the dislocation of the suspension only occurs for concentrated-enough suspensions, and the corresponding minimum volume fraction ranges from less than 2% for 20-μm particles to 20% for 500-μm particles.

Transitions between the Different Thinning Regimes. Fig. 3*A* reports the evolution of the critical thickness $h^\star$ at the transition between the equivalent fluid regime (I) and the dislocation regime (II) when varying the volume fraction ϕ for monodisperse suspensions with different particle diameters. The thickness $h^\star$ increases both with ϕ and d. Indeed, the larger the particles, the larger the thickness $h^\star$ is, and the denser the suspensions, the larger $h^\star$ is. Interestingly, the heterogeneities brought by the particles start occurring at a much larger length scale than the particle diameter. The critical thickness of the transition between the dislocation regime (II) and the interstitial regime (III), h', depends on the particle diameter d but not significantly on the volume fraction, as illustrated in Fig. 3*B*. This observation is consistent with the concept of dislocation since $h^\star$ marks the onset of heterogeneity when the suspension begins to dislocate, whereas h' marks the end of dislocation when the suspension in the neck is so dilute that it cannot be considered a suspension anymore.

Eq. **1** provides a prediction of the critical thickness $h^\star$ as a function of the properties of the suspension. Assuming that before dislocation, the dynamics results from the balance between gravity and the effective viscosity of the suspension, the relevant timescale in the equivalent liquid regime (I) is given by $t^\star = \eta/(\rho\, g\, h^\star)$. By combining this viscous–gravitational timescale with Eq. **1**, we obtain $h^\star/d \sim {\eta_\mathrm{r}}^{1/3}\ (\ell_\mathrm{c}/d)^{2/3}$, where $\ell_\mathrm{c} = \sqrt{\gamma/(\rho g)}$ is the capillary length (1.5 mm for the silicone oil used here). We estimate the relative viscosity of the suspension $\eta_\mathrm{r}(\phi) = \eta(\phi)/\eta_\mathrm{f}$ using the Maron–Pierce correlation (32), $\eta_\mathrm{r}(\phi) = (1-\phi/\phi_\mathrm{c})^{-2}$, with $\phi_\mathrm{c} \simeq 57.8\%$ for the suspensions used here (17). Finally, we obtain the evolution of the critical thickness at the dislocation regime:

$$\frac{h^\star}{d} \sim \left(\frac{\ell_\mathrm{c}}{d}\right)^{2/3} \left(1-\frac{\phi}{\phi_\mathrm{c}}\right)^{-2/3}. \qquad [2]$$

Fig. 3*C* compares the rescaled dislocation threshold $h^\star/d$ with the quantity $(\ell_\mathrm{c}/d)^{2/3}(1-\phi/\phi_\mathrm{c})^{-2/3}$, which includes the two input parameters of our experiments: the particle diameter d and the volume fraction ϕ. We report in Fig. 3*C* the experimental results for all monodisperse suspensions considered in this study. The experimental results collapse onto a master line, which matches Eq. **2** with the prefactor 0.6. The prediction only fails for very dilute suspensions of large particles, shown by the purple points in the lower left of Fig. 3*C*. In this case, the concept of dislocation becomes irrelevant since there are not enough particles in the neck to consider it as homogenous even during the early stage of the pinch-off. The observation that this approach fails only in this most extreme situation emphasizes the robustness of the model, despite the rough assumptions made previously.

The excellent agreement between our experiments and the model demonstrates that the acceleration of the thinning for dense-enough suspensions is indeed induced by the dislocation at the neck. Changing the solvent viscosity and wetting properties from 0.12 Pa×s (silicone oil) to 2.6 Pa×s [poly(ethylene glycol-ran-propylene glycol) monobutyl ether (PEG)] (diamonds in Fig. 3*C*) does not affect the collapse of the data and the agreement between the model and the experiments. We were also able to extract the value $h^\star$ from recent experiments performed by Moon et al. (13), which provided the thinning dynamics for suspensions of 10-μm particles. The model presented in this paper also captures their experimental data (*SI Appendix*).

Similarly to Eq. **2**, we can derive the threshold h' between the dislocation regime (II) and the interstitial regime (III). The typical timescale at this transition is given by $t' \sim \eta_\mathrm{f}/(\rho g h')$. Combining this timescale with Eq. **1** yields

$$\frac{h'}{d} \sim \left(\frac{\ell_\mathrm{c}}{d}\right)^{2/3}. \qquad [3]$$

The corresponding experimental measurements of h' plotted with respect to $(\ell_\mathrm{c}/d)^{2/3}$ for different monodisperse suspensions are reported in Fig. 3*D*. Once again, we obtain an excellent agreement between the model of Eq. **3** and the experimental results. The collapse of the data onto the proposed law provides a second proof that the acceleration of the thinning is caused by the dislocation. Similar to what was observed for $h^\star$, the prediction for h' fails for very dilute suspensions of large particles. In these cases, it is notable that $h^\star$ and h' are very close and smaller than the particle size d. This means that the thinning switches directly from the equivalent regime to the interstitial regime. Indeed, since not enough particles are present in the neck, there is no dislocation mechanism.

Polydisperse Suspensions. Monodisperse suspensions characterized by a single length scale, the diameter d of the particles, are valuable to study due to their simplicity. Nevertheless, actual manufacturing applications or capillary processes primarily involve polydisperse suspensions. In a polydisperse suspension, each possible particle size is theoretically a relevant length scale of the flow. As a first step, we consider the dislocation of bidisperse suspensions. Bidisperse suspensions contain a volume fraction of particles ϕ, split among ϕ_S of small particles of diameter d_S and ϕ_L of large particles of diameter d_L. We introduce the volume ratio of small particles $\xi = \phi_\mathrm{S}/\phi$ and the size ratio of particles $\delta = d_\mathrm{L}/d_\mathrm{S}$ (33). For all of these suspensions and a volume fraction ϕ ranging from 0 to 50%, we observe a thinning dynamic similar to that of the monodisperse case, with the three successive regimes. The main difference is that the thresholds of the dislocation regime, $h^\star$ and h', now depend on the composition parameters, ξ and δ.

Polydisperse suspensions are defined by the size distribution of their particles, which we can be described through a volume-averaged particle diameter $\bar{d}$. For a bidisperse suspension, this quantity is $\bar{d} = \xi d_\mathrm{S} + (1-\xi) d_\mathrm{L}$. The choice of the volume-averaged diameter over the number-averaged diameter will be justified in the last section. In addition to the particle size distribution, polydisperse suspensions also differ by their lower viscosity for a given particle volume fraction than a monodisperse suspension. Indeed, the polydispersity of the particles enables a more efficient filling of the space, described by a larger value of the critical volume fraction $\phi_\mathrm{c}(\xi,\delta)$. The viscosity of a polydisperse suspension can be computed from the jamming fraction of a polydisperse sphere packing using the Maron–Pierce correlation (17, 32), $\eta_\mathrm{r} \sim (1-\phi/\phi_\mathrm{c}(\xi,\delta))^{-2}$, where the critical volume fraction ϕ_c is estimated through the model of Ouchiyama and Tanaka (34). From there, we compute $h^\star$ and h' using $\bar{d}$ and $\phi_\mathrm{c}(\xi,\delta)$ in Eqs. **2** and **3**.

Fig. 4*A* reports the evolution of $h^\star/\bar{d}$ and Fig. 4*B* reports the evolution of $h'/\bar{d}$ compared with the predictions of Eqs. **2**

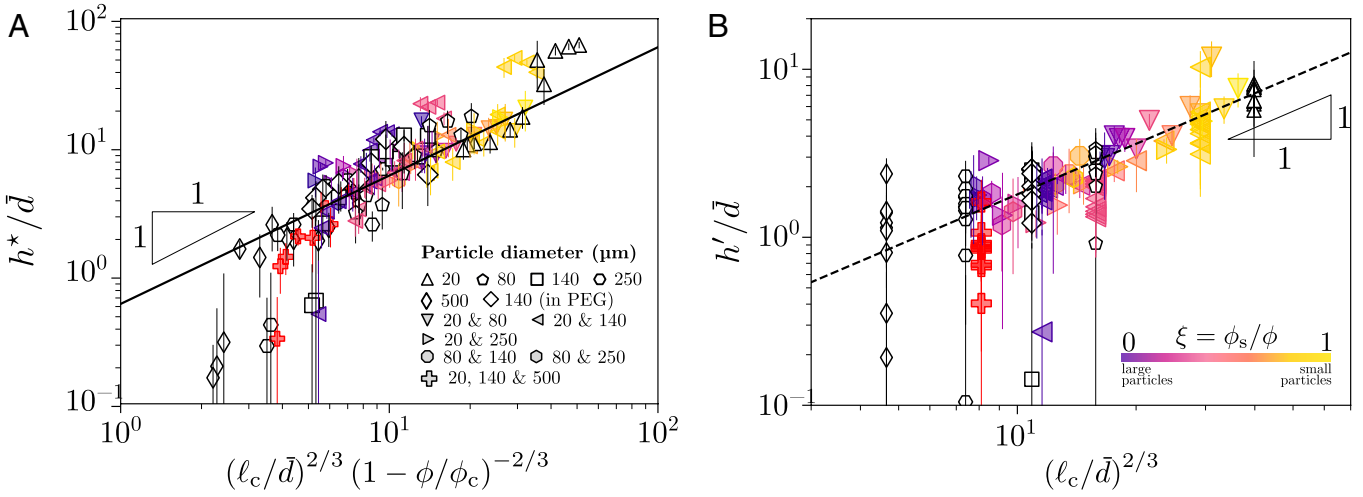

Fig. 4. (*A*) Critical thickness between the equivalent fluid regime (I) and the dislocation regime (II) rescaled by the volume-averaged particle diameter, $h^\star/\bar{d}$, reported following the prediction given by Eq. **2**. (*B*) Critical thickness between the dislocation regime (II) and the interstitial regime (III) rescaled by the particle diameter, $h'/\bar{d}$, plotted following the prediction of Eq. **3**. In both panels, the black open symbols correspond to the monodisperse suspensions presented in Fig. 3, with each symbol shape corresponding to a different particle diameter. The colored symbols represent the results for the polydisperse suspensions, with each symbol corresponding to a couple of particles sizes (in the legend). The colors represent the share of small particles in each suspension ξ from purple for $\xi \to 0$ (large particle–dominated regime) to yellow for $\xi \to 1$ (small particle–dominated regime). The red crosses represent tridisperse suspensions containing one-third 20-μm particles, one-third 140-μm particles, and one-third 500-μm particles. For all suspensions, the volume fraction varies from 2 to 50%. The experiments represented by big diamonds are conducted in PEG, and all the other experiments are performed in silicone oil.

and **3**. The colored symbols represent the bidisperse suspensions, and their color indicates the volume ratio of small particles ξ. The red crosses represent experiments performed with tridisperse suspensions composed of one-third 20-μm particles, one-third 140-μm particles, and one-third 500-μm particles and a total particle volume fraction ϕ ranging from 2 to 50%. The black open symbols represent the monodisperse suspensions, already shown in Fig. 3 *C* and *D*. We show all experiments on the same graph to highlight the universality of our model beyond the simplest monodisperse case usually considered in the literature.

For polydisperse suspensions, the critical thicknesses defining the thresholds of the dislocation regime, $h^\star$ and h', collapse onto the same master line as the monodisperse suspensions. The limitations are the same as in the monodisperse case. More specifically, dilute suspensions of large particles do not dislocate because there are too few particles in the neck. The collapse of h' vs. $\bar{d}$ shown in Fig. 4*B* is even more apparent. Indeed, using a polydisperse suspension allows for tuning the volume-average diameter, and these experiments clarify the dependence of h' on the particle diameter. Therefore, it appears that the dislocation regime only depends on the size distribution through the volume-averaged diameter $\bar{d}$ and the critical volume fraction $\phi_c(\xi, \delta)$.

Discussion

Coherence Length. A notable feature in the pinch-off of suspension drops is that the threshold to the heterogeneous regime $h^\star$ can be much larger than the diameter of the particles d and also depends on the volume fraction ϕ. Indeed, a classical interpretation of the transition between a homogeneous and heterogeneous regime is that the equivalent fluid regime stops when the scale of the flow (here, the neck width h) becomes comparable with the particle size (11, 15). Such an interpretation would lead to $h^\star \sim d$, with a proportionality factor of order one. However, our experiments demonstrate that although for dilute suspensions, $h^\star$ is indeed of the order of the particle diameter, it becomes much larger than d at larger volume fractions. For instance, for $\phi = 50\%$, we measure $h^\star = 1.6$ mm for 140-μm particles, which is more than 11 times the diameter of the particles d. With 20-μm particles, we measure $h^\star = 1.24$ mm, 62 times larger than the particle diameter. More generally, Fig. 3*C* shows that the ratio $h^\star/d$ varies over two orders of magnitude and strongly depends on the volume fraction. The polydisperse suspensions exhibit the same trend, as reported in Fig. 4*A*. Therefore, the heterogeneous structure of dense suspensions plays a role at a scale much larger than the particle diameter. A similar feature has been previously reported for the free surface flow of dense suspensions on an inclined plane. Indeed, Bonnoit et al. (22) have defined a mesoscopic length scale that increases with the volume fraction and diverges at the critical volume transition ϕ_c. The critical thickness $h^\star$ reported in this study is similar and corresponds to the limit of the homogeneous regime, at the onset of heterogeneity. In the present case, this length would also diverge when $\phi \to \phi_c$.

Physically, the length $h^\star$ can be seen as the coherence length of the interactions through which momentum diffuses. As a particle undergoes a fluctuation of its position, it exerts a force upon its neighbors through the lubrication film between them. If there are contacts between particles, they transmit the momentum directly. Other forces can also act on the particles. For instance, for dilute suspension, the viscous drag on the particle should also be taken into account. If the particles are small enough, they will be subject to Brownian motion and van der Waals forces. The coherence length can then be seen as the typical length over which a fluctuation will be damped. Therefore, a stress applied on the suspension will be distributed across a volume defined by the coherence length. In the present configuration, during the detachment of the drop, the curvature of the neck generates a capillary pressure gradient between the neck and the rest of the suspension. The resulting stress will be distributed across the suspension if the neck is thicker than the coherence length. However, if the neck is thinner than the coherence length, a fraction of the suspension may experience larger local stress, which pulls the particles apart from each other and leads to the breakup through dislocation. Therefore, the coherence length here controls the stability of the suspension against a concentration fluctuation.

Here, the words fluctuation and coherence length are meant to suggest an analogy with statistical mechanics, even if it is only a rough sketch. As the suspension flows, each particle creates a local disturbance, and one can imagine an ideal state of local equilibrium where the distance between particles is maximum so the global dissipation is minimum. Deviations from this ground state would be caused by the preparation of the suspension and by the constraints applied on the suspension (shape of the container, stress, body force). There are similarities with this approach and the Edwards ensemble (35, 36), in which the volume fraction of granular media plays the role of energy. For suspensions, volume fraction is directly linked to the rate of dissipation (by the viscosity), which is the quantity that should be minimized.

The correlation length also applies to polydisperse suspensions, although the range of sizes of the particles makes the interactions between particles more complex. Assuming that the volume of the lubrication film around a given particle is directly proportional to the volume of that particle, the lubrication pressure between small particles and between large particles is of different magnitude. This explains why $h^\star$ is relatively much larger for 20-μm particles than for larger particles (Fig. 2*C*). Indeed, for smaller particles, the relative lubrication pressure between them is stronger, and therefore, a perturbation may spread further. Therefore, the coherence length should depend not only on the number of interactions but also, on the relative force of these interactions. As a result, the relevant length scale of polydisperse suspensions is the volume-averaged diameter rather than the number-average diameter. Similarly, the Ouchiyama–Tanaka model (34) with which we compute ϕ_c for the polydisperse suspensions is based on a volume average of the local volume fraction. Therefore, the pinch-off dynamics, particularly the transition between the different regimes, of a polydisperse suspension can be inferred from the volume-averaged particle diameter and volume-averaged volume fraction.

Our pinch-off experiments with bidisperse suspensions reveal that they follow dynamics similar to monodisperse suspensions, meaning that pinch-off does not filter particles by size. The dislocation model enables us to understand why; despite the size difference, the movement of small particle remains strongly correlated to that of large particles, and they are not easily separated. This good agreement of our model with the bidisperse suspensions enable us to neglect self-filtration (37, 38) as a mechanism for the accelerated pinch-off.

Two-Particle Interaction. Contrarily to $h^\star$, the length h' does not depend much on the volume fraction ϕ (Fig. 3*C*). From a neck thickness $h(t) = h'$ and smaller, the neck reduces to a filament of interstitial liquid, without any particle in it. Just before this transition, the neck contains two particles, and the film between them experiences all of the stress acting on the neck. Thus, h' can be interpreted as the thickness that balances the viscous interaction between the last two particles of the neck and the driving force of the thinning (capillarity and the weight of the drop in the present case).

Multiple Dislocations. Various studies on the pinch-off of suspension have reported qualitatively similar results. In particular, the pinch-off of suspension drops from other studies should also be explained by the mechanisms and scaling law presented in this work (18, 19). In both studies, the thinning of the suspension was empirically interpreted in terms of non-Newtonian rheology. We demonstrate in the following that the concept of dislocation can explain these results without involving a non-Newtonian rheology.

Roché et al. (18) studied the thinning of cornstarch suspensions in water, with an average particle diameter of 14-μm. For $\phi = 37\%$, they observed a long filament that would eventually destabilize into "jammed" regions where the strain rate was zero and "flowing" regions where the thinning continues. They measured the wavelength between two flowing regions as 700-μm, although the theory of the Rayleigh–Plateau instability predicts 7 mm. Applying Eq. **2** to their configuration ($d = 14\mu\text{m}$, $\ell_c = 2.7$ mm for water), we obtain $628\text{-}\mu\text{m} < h^\star < 875\mu\text{m}$ in their range of volume fraction ($23\% < \phi < 39\%$). Thus, if the length of the neck is much longer than $h^\star$ when $h(t) = h^\star$, several dislocations can happen simultaneously, and $h^\star$ is then the wavelength of the destabilization. Although the authors considered the regions not thinning as jammed, it does not necessarily need to be the case, and the thinning simply continues where the viscosity is the lowest (i.e., in the dislocating regions). Pan et al. (19) studied denser suspensions of smaller particles ($1.3\,\mu\text{m} \leq d \leq 10\,\mu\text{m}$, with $55\% \geq \phi \geq 59\%$). The thinning dynamics of their aqueous suspensions are similar to those of our viscous liquids; however, they did not observe dislocation. In their configuration, the coherence length of their suspensions, calculated through Eq. **2**, is a few millimeters depending on the jamming fraction. The filament is then always shorter than the wavelength of the destabilization and is, therefore, stable.

Dislocation of Capillary Bridges. In a recent study, Château et al. (29) observed the pinching and breakup of capillary bridges of suspensions. Although their configuration is different from a pending drop, they also reported a deviation from the homogeneous liquid regime but did not provide a model to explain the variations of $h^\star$. The scaling law for the thinning regime (Eq. **1**) matches their data for $\phi > 20\%$, whereas a linear law fits better for $\phi \leq 20\%$ (*SI Appendix*). Therefore, it seems that by plotting the last moments of the dynamics, Château et al. (29) were observing the interstitial regime for $\phi \leq 20\%$ and the dislocation regime for $\phi > 20\%$. In the latter case, the interstitial regime may have been too short to be observed. However, their empirical scaling for $h^\star$ differs from ours, probably because the flow is different.

Conclusion

The pinch-off of a drop of particulate suspension undergoes three regimes: first, the equivalent liquid regime followed by a dislocation regime and finally, the interstitial regime. In the first regime, the drop of suspension behaves like a drop of a homogeneous liquid of matching viscosity, and the particles simply rearrange when the drop deforms; this is the equivalent liquid regime. Below a certain thickness of the neck, $h^\star$, the particles cannot simply rearrange themselves and start moving away from each other; the suspension dislocates. Finally, when particles are too far from each other to interact, the neck reduces to a filament of interstitial liquid. This is the interstitial regime, identical to the viscous-capillary regime observed during the pinch-off of a viscous liquid. This last transition occurs at the thickness h', representing the interaction range between two particles.

The dislocation of the suspension is caused by the amplification of a fluctuation of local volume fraction. We obtained in this study a scaling law for this regime, $h(t) \sim (t_c - t)^{1/2}$, as well as for the critical thicknesses $h^\star$ and h'. These predictions captured all experiments, including those performed with polydisperse suspensions. The critical length $h^\star$ translates the balance between the driving force of the interactions between the particles. This length corresponds to a coherence length of the suspension under the stress caused by capillary pressure and the weight of the falling drop.

Although our experiments considered the detachment of a drop, the concepts of coherence length and dislocation developed here go beyond this particular situation and should apply to other suspension flow. Notably, the flow of suspensions on an inclined plane exhibits a similar length scale, much larger than the particle diameter, and defines the threshold from the effective liquid regime to an intermediate regime (22). Therefore, it appears that the onset of heterogeneity in the flows of suspensions is controlled not directly by the size of the particles but by the reach of the long-range interactions between them.

In conclusion, two length scales that depend on the particle diameter d and the volume fraction ϕ characterize the capillary flow of suspension: the reach of the interactions between two particles and the coherence length of these interactions across the suspension. Since the interactions occur because of external stress, these length scales themselves depend on this applied stress. Future studies will apply these concepts to other systems involving suspensions, such as the formation of thin films (23, 24, 25) and the fragmentation of suspension ligaments and sheets (26). In addition, beyond polydisperse suspensions, the dislocation of other kinds of complex suspensions (for example, made of nonspherical particles, such as fibers, or even active particles) should be considered. We expect that exploring different flows will enable a better comprehension of the interactions between particles that can lead to more predictive manufacturing processes.

Materials and Methods

Particulate Suspensions. The suspensions are made of polystyrene particles (DynoSeeds from Microbeads) with measured diameters of 21.6 $\pm$ 0.9, 80.3 $\pm$ 5.0, 144.2 $\pm$ 8.3, 249.0 $\pm$ 4.2, and 578.1 $\pm$ 10.1 μm. These particles are referred to in the article as 80, 140, 250, and 500-μm, respectively. The roughness of the particles is of order 100 nm (39), and their density is in the range $\rho = 1050 - 1060$ kg/m^3. The particles are dispersed in a density-matched interstitial liquid to prevent buoyancy effects. We primarily used AP100 silicone oil (from Sigma Aldrich) of shear viscosity $\eta_f = 120$ mPa$\times$s and surface tension $\gamma = 24 \pm 2$ mN/m at 20 $^\circ$ C, which perfectly wets the particle. We also conducted experiments with particles dispersed in PEG (Sigma Aldrich), for which $\eta_f = 2.5$ Pa$\times$s and $\gamma = 45$ mN/m. The molar weight being as low as 3,900 g/mol, this solvent can be considered Newtonian. For both interstitial liquids used in this study, the settling time of the particles is much longer than the timescale of the experiments so that the suspensions can be considered as neutrally buoyant.

The bidisperse suspensions are composed of the same interstitial fluid (silicone oil AP100) and made using a couple of particle sizes (d_S, d_L) chosen among (20, 80-μm), (20, 140-μm), (20, 250-μm), (80, 140-μm), and (80, 250-μm). In these experiments, we also vary the volume fraction of small particles $\xi = \phi_S/(\phi_S + \phi_L)$. The tridisperse suspensions contains one-third 20-μm particles, one-third 140-μm particles, and one-third 500-μm particles.

Pinch-Off Experiments. The suspensions are transferred to a syringe and then manually extruded through a nozzle of outer diameter 2.75 mm (for wetting liquids, the outer diameter is the relevant length scale). The extrusion is conducted slowly to avoid any inertial effects. The experiments are recorded using a high-speed camera (Phantom VEO 710) equipped with a macro lens (Nikon Micro-Nikkor 200-mm AI-S). To resolve perfectly the contour of the drop and the filament, we place a panel of light emitting diodes (LEDs, from Phlox) behind the experimental setup. The time evolution of the contour of the drop and the minimum diameter of the filament $h(t)$ are extracted through custom-made routines using ImageJ and Python.

Rescaling and Relevant Lengths. To measure $h^\star$, we rescale the time as $\alpha_\eta(t_c - t) + \Delta t$ and find the critical thickness at which the rescaled dynamics of the suspension deviates from the dynamics of the interstitial liquid. The stretching parameter α_η accounts for the viscosity difference between the suspension and the Newtonian liquid used for comparison. The time shift Δt accounts for the acceleration of the thinning due to the presence of the particles. Previous work at constant volume fraction ϕ suggested that α_η can be seen as the viscosity ratio between the suspension and the comparative Newtonian liquid $\eta_r = \eta/\eta_f$ (17). However, the present study shows that this result does not hold if the difference in viscosity between the suspensions and the viscous liquid used for comparison is too large. Although α_η follows the same divergence as the viscosity, the evolution of α_η over a broad range of volume fraction ϕ does not quantitatively match the viscosity of the suspensions measured with a rheometer. The length $h^\star$ is the thickness at which the rescaled dynamics of the suspension deviates from that of the interstitial fluid. We defined it systematically as the point where the thinning rate dh/dt of the suspension differs by more than 5% from that of the interstitial liquid. The length h' (smaller than $h^\star$) is defined as the thickness at which the thinning dynamics of the filament becomes linear (i.e., follows a capillary-viscous regime).

Dislocation. To describe the dislocation regime, we consider the stretching of a liquid film of thickness a between two portions of suspension pulled apart at the velocity $\dot{a}$. We estimate the power dissipated in the flow within. Assuming that the suspension on each side of the film is much more viscous than the interstitial liquid ($\eta_r \gg 1$), we approximate the flow as that of two plates pulled apart. The liquid film is then set between two cylindrical plates of diameter h at positions $z = 0$ and $z = a$. By solving the Stokes equation in the lubrication approximation, we obtain the axial velocity gradient:

$$\frac{\partial u_r}{\partial z} = 3\frac{\dot{a}}{a^3} r(2z - a). \qquad [4]$$

We integrate the velocity gradient over the volume of the film and obtain the order of magnitude for the power of viscous dissipation in the neck:

$$\mathcal{P}_{\text{dis}} = \iiint_\Omega \eta_f \left(\frac{\partial u_r}{\partial z}\right)^2 d\Omega \sim \eta_f \frac{h^4}{a^3}\dot{a}^2. \qquad [5]$$

Data Availability. All study data are included in the article and/or supporting information.

ACKNOWLEDGMENTS. This material is based upon work supported by NSF Faculty Early Career Development (CAREER) Program Award Chemical, Bioengineering, Environmental and Transport Systems (CBET) 1944844 and American Chemical Society Petroleum Research Fund Grant 60108-DNI9. We thank C. Josserand for helpful discussions.

1. M. M. Denn, J. F. Morris, Rheology of non-Brownian suspensions. *Annu. Rev. Chem. Biomol. Eng.* **5**, 203–228 (2014).
2. J. R. Castrejón-Pita *et al.*, Plethora of transitions during breakup of liquid filaments. *Proc. Natl. Acad. Sci. U.S.A.* **112**, 4582–4587 (2015).
3. A. Lagarde, C. Josserand, S. Protière, Oscillating path between self-similarities in liquid pinch-off. *Proc. Natl. Acad. Sci. U.S.A.* **115**, 12371–12376 (2018).
4. J. M. Montanero, A. M. Gañán-Calvo, Dripping, jetting and tip streaming. *Rep. Prog. Phys.* **83**, 097001 (2020).
5. J. Eggers, E. Villermaux, Physics of liquid jets. *Rep. Prog. Phys.* **71**, 036601 (2008).
6. B. Derby, Inkjet printing of functional and structural materials: Fluid property requirements, feature stability, and resolution. *Annu. Rev. Mater. Res.* **40**, 395–414 (2010).
7. D. Lohse, Fundamental fluid dynamics challenges in inkjet printing. *Annu. Rev. Fluid Mech.* **54**, 349–382 (2022).
8. S. V. Murphy, A. Atala, 3D bioprinting of tissues and organs. *Nat. Biotechnol.* **32**, 773–785 (2014).
9. Y. Amarouchene, D. Bonn, J. Meunier, H. Kellay, Inhibition of the finite-time singularity during droplet fission of a polymeric fluid. *Phys. Rev. Lett.* **86**, 3558–3561 (2001).
10. V. Thiévenaz, A. Sauret, Pinch-off of viscoelastic particulate suspensions. *Phys. Rev. Fluids* **6**, L062301 (2021).
11. R. J. Furbank, J. F. Morris, An experimental study of particle effects on drop formation. *Phys. Fluids* **16**, 1777–1790 (2004).
12. C. Bonnoit, T. Bertrand, E. Clément, A. Lindner, Accelerated drop detachment in granular suspensions. *Phys. Fluids* **24**, 043304 (2012).
13. J. Y. Moon, S. J. Lee, K. H. Ahn, S. J. Lee, Filament thinning of silicone oil/poly (methyl methacrylate) suspensions under extensional flow. *Rheol. Acta* **54**, 705–714 (2015).
14. M. S. van Deen *et al.*, Particles accelerate the detachment of viscous liquids. *Rheol. Acta* **52**, 403–412 (2013).
15. R. J. Furbank, J. F. Morris, Pendant drop thread dynamics of particle-laden liquids. *Int. J. Multiph. Flow* **33**, 448–468 (2007).
16. A. Lindner, J. E. Fiscina, C. Wagner, Single particles accelerate final stages of capillary break-up. *Europhys. Lett.* **110**, 64002 (2015).
17. V. Thiévenaz, S. Rajesh, A. Sauret, Droplet detachment and pinch-off of bidisperse particulate suspensions. *Soft Matter* **17**, 6202–6211 (2021).

18. M. Roché, H. Kellay, H. A. Stone, Heterogeneity and the role of normal stresses during the extensional thinning of non-Brownian shear-thickening fluids. *Phys. Rev. Lett.* **107**, 134503 (2011).
19. Z. Pan, N. Louvet, Y. Hennequin, H. Kellay, D. Bonn, Drop formation in shear-thickening granular suspensions. *Phys. Rev. E Stat. Nonlin. Soft Matter Phys.* **92**, 052203 (2015).
20. M. Z. Miskin, H. M. Jaeger, Droplet formation and scaling in dense suspensions. *Proc. Natl. Acad. Sci. U.S.A.* **109**, 4389–4394 (2012).
21. C. McIlroy, O. G. Harlen, Modelling capillary break-up of particulate suspensions. *Phys. Fluids* **26**, 033101 (2014).
22. C. Bonnoit, J. Lanuza, A. Lindner, E. Clement, Mesoscopic length scale controls the rheology of dense suspensions. *Phys. Rev. Lett.* **105**, 108302 (2010).
23. S. Palma, H. Lhuissier, Dip-coating with a particulate suspension. *J. Fluid Mech.* **869**, R3 (2019).
24. A. Gans *et al.*, Dip-coating of suspensions. *Soft Matter* **15**, 252–261 (2019).
25. D. Jeong, M. Lee, V. Thiévenaz, M. Bazant, A. Sauret, Dip coating of bidisperse particulate suspensions. *J. Fluid Mech.*, **936**, A36 (2022).
26. P. S. Raux, A. Troger, P. Jop, A. Sauret, Spreading and fragmentation of particle-laden liquid sheets. *Phys. Rev. Fluids* **5**, 044004 (2020).
27. J. Château, H. Lhuissier, Breakup of a particulate suspension jet. *Phys. Rev. Fluids* **4**, 012001 (2019).
28. M. Zhao *et al.*, Spreading of granular suspensions on a solid surface. *Phys. Rev. Res.* **2**, 022031 (2020).
29. J. Château, É. Guazzelli, H. Lhuissier, Pinch-off of a viscous suspension thread. *J. Fluid Mech.* **852**, 178–198 (2018).
30. J. Eggers, Universal pinching of 3D axisymmetric free-surface flow. *Phys. Rev. Lett.* **71**, 3458–3460 (1993).
31. D. T. Papageorgiou, On the breakup of viscous liquid threads. *Phys. Fluids* **7**, 1529–1544 (1995).
32. É. Guazzelli, O. Pouliquen, Rheology of dense granular suspensions. *J. Fluid Mech.* **852**, P1 (2018).
33. A. P. Shapiro, R. F. Probstein, Random packings of spheres and fluidity limits of monodisperse and bidisperse suspensions. *Phys. Rev. Lett.* **68**, 1422–1425 (1992).
34. N. Ouchiyama, T. Tanaka, Porosity of a mass of solid particles having a range of sizes. *Ind. Eng. Chem. Fundam.* **20**, 66–71 (1981).
35. S. F. Edwards, R. Oakeshott, Theory of powders. *Phys. A Stat. Mech. Appl.* **157**, 1080–1090 (1989).
36. A. Baule, F. Morone, H. J. Herrmann, H. A. Makse, Edwards statistical mechanics for jammed granular matter. *Rev. Mod. Phys.* **90**, 015006 (2018).
37. M. D. Haw, Jamming, two-fluid behavior, and "self-filtration" in concentrated particulate suspensions. *Phys. Rev. Lett.* **92**, 185506 (2004).
38. S. D. Kulkarni, B. Metzger, J. F. Morris, Particle-pressure-induced self-filtration in concentrated suspensions. *Phys. Rev. E Stat. Nonlin. Soft Matter Phys.* **82**, 010402 (2010).
39. A. Deboeuf, G. Gauthier, J. Martin, Y. Yurkovetsky, J. F. Morris, Particle pressure in a sheared suspension: A bridge from osmosis to granular dilatancy. *Phys. Rev. Lett.* **102**, 108301 (2009).

PNAS
www.pnas.org

Supplementary Information for

The onset of heterogeneity in the pinch-off of dense suspensions drops

Virgile Thiévenaz and Alban Sauret

E-mail: asauret@ucsb.edu

This PDF file includes:

Supporting Information Text

1. Videos

The videos listed below correspond to the images shown in Figure 1. Movies 3 and 4 are also given with the velocity field overlayed. The velocity field is calculated using the ImageJ PIV analysis plugin; high velocities are shown in red, medium in green, low in purple. These videos reveal that in the dislocation regime, the velocity gradient (represented by a sharp change of color)is very localized in the neck. Hence, the thinning occurs mainly in the neck, and not in the rest the drop.

Movie 1: Pinch-off of a drop of silicone oil, without particles. This video corresponds to the pictures in Figure 1a. Play speed in 100 times slower than the real pinch-off.

Movie 2: Pinch-off of a drop of suspension of 2% of 140μm particles in silicone oil. This video corresponds to the pictures in Figure 1b. Play speed in 100 times slower than the real pinch-off.

Movie 3: Pinch-off of a drop of suspension of 20% of 140μm particles in silicone oil. This video corresponds to the pictures in Figure 1c. Play speed in 100 times slower than the real pinch-off.

Movie 3 PIV: Same as Movie 3, with the velocity field overlaid. Play speed in 100 times slower than the real pinch-off.

Movie 4: Pinch-off of a drop of suspension of 50% of 140μm particles in silicone oil. This video corresponds to the pictures in Figure 1d. Play speed in 100 times slower than the real pinch-off.

Movie 4 PIV: Same as Movie 4, with the velocity field overlaid. Play speed in 100 times slower than the real pinch-off.

Movie 5: Pinch-off of a drop of suspension of 50% of 20μm particles in silicone oil. This video corresponds to the pictures in Figure 1e. Play speed in 100 times slower than the real pinch-off.

Movie 6: Pinch-off of a drop of suspension of 50% of 250μm particles in silicone oil. This video corresponds to the pictures in Figure 1f. Play speed in 100 times slower than the real pinch-off.

2. Shape of the drop

A key hypothesis in our model is that the dislocation is a local process. Fig. S1 shows the time evolution of the contour of a drop of suspension during pinch-off, for $\phi = 40\%$ and $d = 140\mu$m. The three thinning regimes are easily separated, with critical time $t^\star$ and t' corresponding to critical thicknesses: $h(t^\star) = h^\star$ and $h(t') = h'$. In the homogeneous regime, the thinning of the neck is part of a global deformation of the drop, as can be seen in Fig. S1(a). Conversely, the dislocation regime corresponds to a local thinning, driven by the fall of the drop (with also a role of capillary forces) and is reported in Fig. S1(b). The suspension that is above the neck does not flow anymore; the suspension below moves but does not deform significantly, leading to a local effect. Finally, the interstitial regime is also localized at the neck where no particles are present, and is driven by capillary forces only. In this case, only the neck deforms, as shown in Fig. S1(c).

Fig. S2 reports the time evolution of the position of the thinnest point z at which h is measured, for different volume fractions ϕ [Fig. S2(a)] and for different particle diameters [Fig. S2(b)]. In all but one case, the movement of the neck is a continuous and monotonous fall. The only exception is for very dilute suspensions ($\phi = 2\%$, purple points in the inset of Fig. S2(a)). In this case, shortly before the pinch-off, the neck rises back up, similarly to the pure liquid case. We should emphasize that we do not observe any change in the z-dynamics when the dislocation starts. This is probably because the corresponding decrease in viscous dissipation at the neck is too weak to really impact the fall of the drop. Once again, it shows that the dislocation is a local phenomenon that mainly occurs in the neck.

3. The Ouchiyama-Tanaka model: maximum packing of polydisperse particles

We consider a packing of spheres having N possible diameters x_i, so that $x_1 < \ldots < x_i < \ldots < x_N$. The non-dimensionalized diameter δ_i is defined relatively to the largest diameter: $\delta_i = x_i/x_N$. The total particle volume fraction is ϕ, each size of particle taking a fraction ξ_i so that the volume fraction of particles of size x_i is $\xi_i\phi$. The packing contains N_i particles of size x_i, and we define the number fraction $f_i = N_i/N$ as

$$f_i = \frac{\xi_i/\delta_i}{\sum_{j=1}^{N} \xi_j/\delta_j}. \quad [1]$$

The number-averaged diameter is then given by

$$\bar{\delta} = \sum_{i=1}^{N} \delta_i f_i. \quad [2]$$

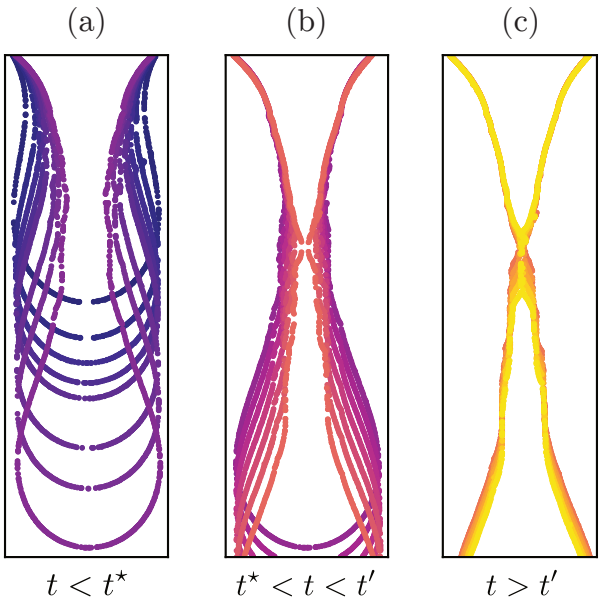

Fig. S1. Time evolution of the contour of the drop for $\phi = 40\%$ and $d = 140\mu$m. The contour is extracted from the experiment shown in Figure 2(c) in the main article. (a) Evolution in the homogeneous regime (for h > $h^\star$). (b) Evolution in the dislocation regime (for h' > h > h'). (c) Evolution in the interstitial regime (for h < h'). The colors represent the time evolution, elapsing from purple to yellow.

According to the calculations of Ouchiyama and Tanaka (1), the jamming fraction of the packing is given by:

$$\phi_c = \frac{\sum_{i=1}^{N} {\delta_i}^3 f_i}{\sum_{i=1}^{N} \left((\delta_i \sim \bar{\delta})^3 + \frac{(\delta_i + \bar{\delta})^3 - (\delta_i \sim \bar{\delta})^3}{\bar{n}} \right)}, \quad [3]$$

with

$$\bar{n} = 1 + \frac{4}{13}(8\phi_0 - 1)\,\bar{\delta} \frac{\sum_{i=1}^{N} (\delta_i + \bar{\delta})^2 \left(1 - \frac{3}{8}\frac{\bar{\delta}}{\bar{\delta} + \delta_i}\right) f_i}{\left[{\delta_i}^3 - (\delta_i \sim \bar{\delta})^3\right] f_i}, \quad [4]$$

and where we have used the notation

$$x \sim y = x - y \quad \text{if } x > y \quad [5]$$
$$= 0 \quad \text{if } x \leq y. \quad [6]$$

The prediction given by Eqs. [3]-[4] is limited, however, by the asymptotical expression for $\delta \to \infty$: $\phi_c(\xi, \delta \to \infty) = \phi_0/(1-\xi)$, which describes a packing where infinitely small particles occupy all the space available between the large particles. Indeed, the bidisperse packing cannot be more compact. Therefore, for a given distribution of particle size, we compute $\phi_c(\xi, \delta)$ through Eqs. [3]-[4], and if is greater than $\phi_0/(1-\xi)$, we correct it back to $\phi_0/(1-\xi)$.

4. More dislocation

In 2015, Moon *et al.* studied experimentally the pinch-off of suspension drops. We extracted the thinning dynamics from their experiments performed with 10 μm PMMA particles dispersed in silicone oil. We were able to measure the length $h^\star$ for three of them (ϕ =10, 15, and 20%). Figure S4 reports the resulting data points (shown in color circles) compared to the result of the experiments performed in the present work (black symbols). These data, obtained in an independent study, collapse perfectly on the master curve corresponding to Eq. [2] in the main article. Therefore, we can extend the range of applicability of the model developed in the present work down to 10μm-particles.

In 2018, Château *et al.* (3) studied the pinch-off of capillary bridges of suspensions. Although this configuration is slightly different from the pinch-off of droplets considered here, they observed a specific thinning regime for volume fractions larger than 20%, but did not provide a model to rationalize these measurements. Figure S5 shows data from Fig. 12(b) of their paper, replotted with the scaling law for the thinning dynamics in the dislocation regime (Eq. [1] in the main article): $h \sim (t_c - t)^{1/2}$. Therefore, it suggests that Château *et al.* were observing the interstitial thinning regime for dilute suspensions and the dislocation for denser ones.

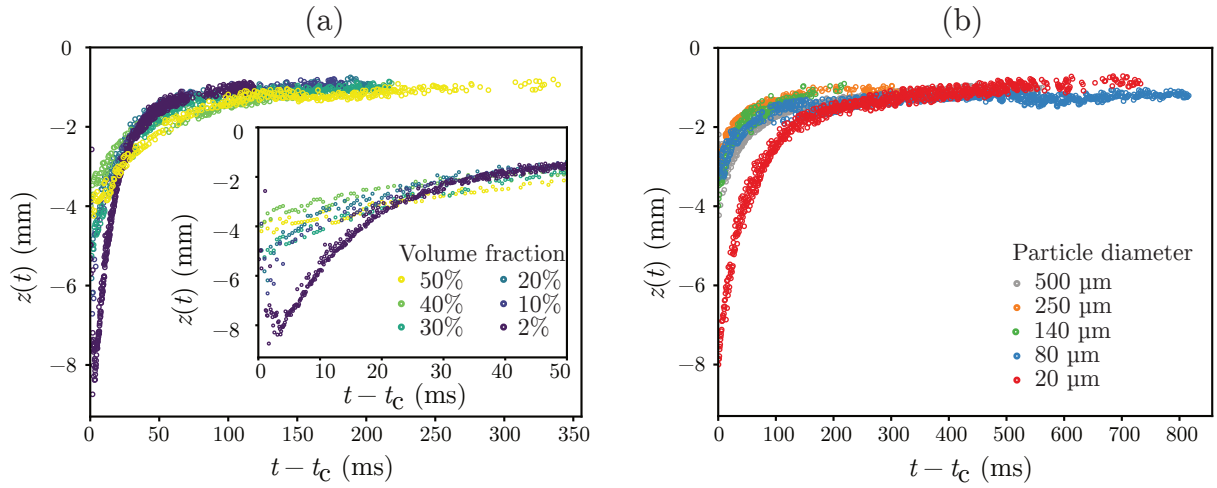

Fig. S2. Time evolution of the vertical position of the thinnest diameter for (a) 140μm particles and various volume fraction ϕ; (b) various particle diameter at 50% volume fraction. The inset in (a) zooms in on the last instants before pinch-off.

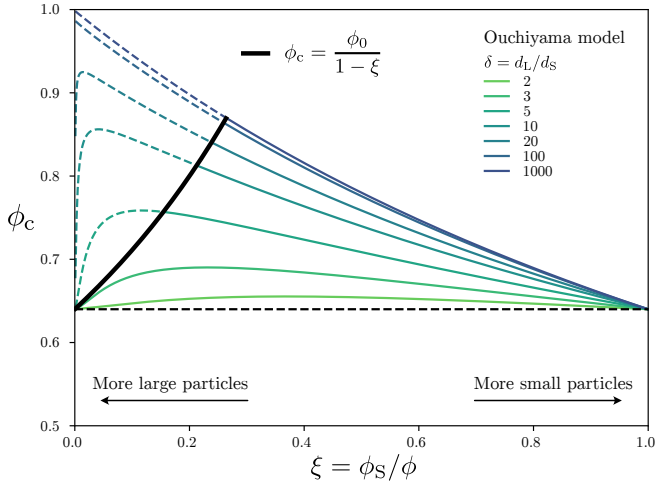

Fig. S3. Predictions for $\phi_c(\xi, \delta)$ used in the main article, shown for an arbitrary value of $\phi_0 = 0.64$. Colored lines show predictions for different size ratios δ, according to the Ouchiyama-Tanaka model (Eqs. [3]-[4]), from 2 (green) to 1000 (purple). Each curve is separated between a physical part (solid line) and a non-physical part (dashed line) depending on whether the predicted ϕ_c is greater or lesser than the optimal packing fraction. The optimal packing fraction for a given ξ, which equals $\phi_c = \frac{\phi_0}{1-\xi}$, is plotted as a thick black line.

References

1. N Ouchiyama, T Tanaka, Porosity of a mass of solid particles having a range of sizes. *Ind. & Eng. Chem. Fundamentals* **20**, 66–71 (1981).
2. JY Moon, SJ Lee, KH Ahn, SJ Lee, Filament thinning of silicone oil/poly (methyl methacrylate) suspensions under extensional flow. *Rheol. Acta* **54**, 705–714 (2015).
3. J Château, É Guazzelli, H Lhuissier, Pinch-off of a viscous suspension thread. *J. Fluid Mech.* **852**, 178–198 (2018).

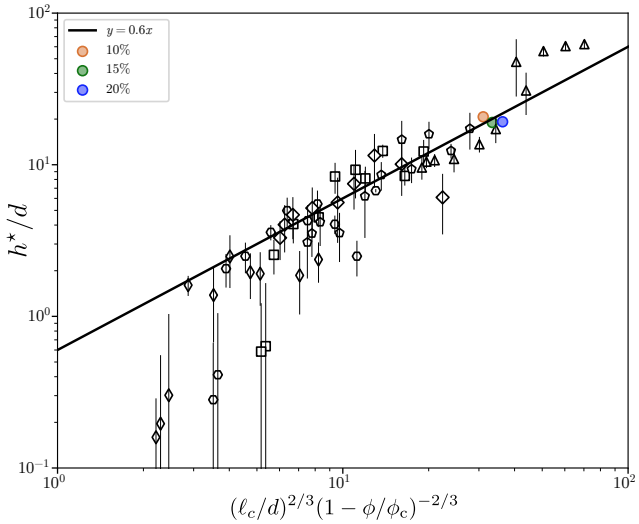

Fig. S4. Data from Figure 3(c) (open black symbols), replotted to compare with the measurements extracted from Moon et al. (2) (colored symbols).

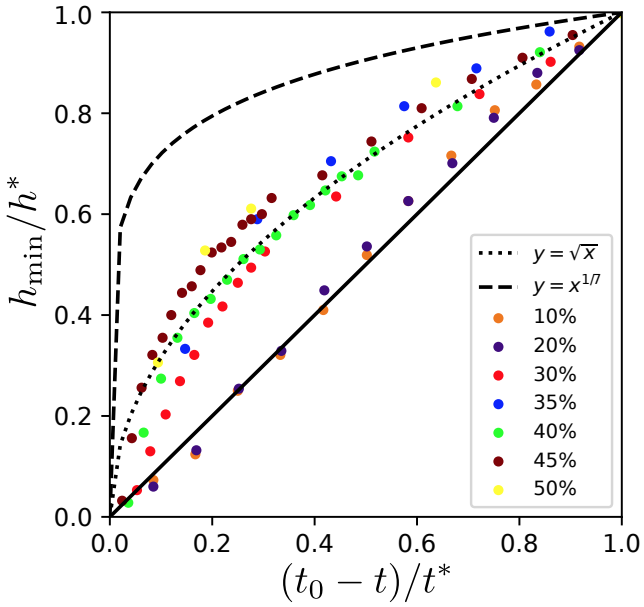

Fig. S5. Figure 12(b) of Château *et al.* (3), replotted with the scaling law $h \sim (t_0 - t)^{1/2}$ (dotted line). The solid line shows the linear thinning for dilute suspensions, the dashed line shows the power law $h \sim (t_0 - t)^{1/7}$ provided by the authors.